Investigating Subglacial Water-filled Cavities by Spectral Analysis of Ambient Seismic Noise: Results on the Polythermal Tête-Rousse Glacier (Mont Blanc, France)

Antoine Guillemot, N Bontemps, E Larose, D Teodor, S Faller, L Baillet, S Garambois, E Thibert, O Gagliardini, Christian Vincent

Investigating Subglacial Water-filled Cavities by Spectral Analysis of Ambient Seismic Noise: Results on the Polythermal Tête-Rousse Glacier (Mont Blanc, France)

A. Guillemot[1,2], N. Bontemps[1], E. Larose[1], D. Teodor[1], S. Faller[1,3], L. Baillet[1], S. Garambois[1], E. Thibert[4], O. Gagliardini[4] and C. Vincent[4]

[1] ISTerre, Université Grenoble Alpes, Université Savoie Mont-Blanc, CNRS, IRD, Université Gustave Eiffel, France

[2] Géolithe, Géolithe Innov, Crolles, France

[3] EOST Strasbourg, France

[4] IGE, Université Grenoble Alpes, CNRS, IRD, INRAE, G-INP, Grenoble, France

Corresponding author: Antoine Guillemot (antoine.guillemot@univ-grenoble-alpes.fr)

Key Points:

- Spectral analysis from ambient seismic noise is complementary to other geophysical methods for investigating glaciers at depth
- Results suggest that the vertical-to-horizontal spectral ratio (VHSR) is a reliable proxy to locate subglacial cavities
- Experimental results were confirmed using a simplified numerical model

Abstract

Polythermal glaciers can trap considerable volumes of liquid water with the potential to generate devastating outburst floods. This study aims to identify water-filled subglacial reservoirs from ambient seismic noise collected by moderate-cost surveys. The horizontal-to-vertical spectral ratio (HVSR) technique is highly sensitive to impedance contrasts at interfaces, thus commonly used to estimate glacier thickness. Here, we focus on the inverse ratio, i.e., the V/H spectral ratio (VHSR), whose high values indicate a low impedance volume beneath the surface, suggesting subglacial cavities. We analyze VHSR peaks from a seismic array of 60 nodes installed on the Tête-Rousse Glacier (Mont Blanc massif, French Alps); data were gathered over 15 days. Mapping the VHSR amplitude over the free surface reveals the main cavity locations and the basal areas affected by melting within the glacier. Results obtained in the field are supported by a conceptual model based on 3D finite-element simulations.

Plain Language Summary

Considerable volumes of liquid water may be trapped within cavities in polythermal glaciers. If these cavities rupture, the resulting outburst flood has the potential to cause devastation in populated mountain areas. With the aim of testing methods to locate such cavities, we installed 60 small 3-component seismic sensors on the Tête-Rousse Glacier (Mont Blanc massif, French Alps), which is known to contain such cavities. We used these sensors to test a detection method based on ambient seismic noise. For 3 weeks, the sensors recorded vibrations within the glacier. On a glacier without cavities, these vibrations ought to be predominantly in the horizontal direction. In the presence of a cavity, we expect the ice above the cavity to vibrate mostly vertically – like a bridge. In this paper, we highlight areas on the glacier where vertical vibrations were stronger than horizontal vibrations. These areas fit well with the locations of the main known cavities in this glacier, and with areas affected by basal melting. We supported our field observations with modeling based on 3D simulations, paving the way to a new method to locate water-filled cavities within glaciers.

1 Introduction

Subglacial cavities may trap a considerable liquid water content. Within glaciers meltwater reservoirs can be created by a number of factors, such as topographical traps, heterogeneous

thermal flux regimes, variability of seasonal meteorological conditions and, consequently, hydraulic pressure gradients (Björnsson, 1998; Vincent et al., 2010). An unexpected and instantaneous release of water from intraglacial or subglacial cavities (Haeberli et al., 1989; Vincent et al., 2010), known as a glacial outburst flood, often causes avalanches of ice and debris flows (Breien et al., 2008; Cenderelli et al., 2003; Kattelmann et al., 2003; Kershaw et al., 2005; Vilimek et al., 2005), leading to devastating damages in densely populated mountain areas (e.g., Haeberli, 1983). Excavation and drainage processes to evacuate subglacial water-filled cavities remain under-studied (Fountain & Walder, 1998; Boon & Sharp, 2003; Roberts, 2005; Vincent et al., 2010).

Several studies have attempted to identify intraglacial cavities early during their formation (Haeberli et al., 2001, 2002; Vincent et al., 2010; Werder et al., 2010; Gagliardini et al., 2011) with the aim of preventing and mitigating the related hazards. Both active and passive geophysical methods have been deployed to investigate the glacier-bedrock interface and to characterize the physics of glaciers (e.g., Petrenko & Whitworth, 2002). Some commonly used active methods are Ground Penetrating Radar (GPR), seismic refraction, and borehole measurements. In addition, passive seismic techniques can provide a reliable estimation of the seismic properties linked to glacier morphology by measuring ambient seismic noise. By using efficient survey logistics, these passive seismic measurements come at a contained cost (Sergeant et al., 2020). Ambient noise studies have also been successfully used to reveal water flow activity (e.g., Björnsson, 1998; Harper et al., 2010; Helmstetter et al., 2015 a, b; Gimbert et al., 2021; Nanni et al., 2021, 2022). The horizontal-to-vertical-spectral ratio (HVSR) technique, first applied to ambient noise recordings by Nogoshi & Igarashi (1971) and Nakamura (1989), is based on the analysis of H/V frequency content, obtained by dividing the vectorial sum of the horizontal components by the vertical components of the Fourier amplitude for the recorded wavefield. When impedance contrasts exist at interfaces (e.g., a soft layer over a hard bedrock), incident body waves (P-waves, horizontal and vertical S-waves) generate surface (Rayleigh and Love) waves that remain trapped within the shallow layer. When the wavelengths of the incident waves are comparable to the layer's thickness, resonance effects occur. Consequently, the resulting surface waves may have a much larger amplitude than the incident waves (e.g., Picotti et al., 2017). In most cases where a 1D soft layer is underlying a stiffer one, the shape of HVSR curve is primarily determined by the fundamental-mode Rayleigh wave (Konno & Ohmachi, 1998). Under reasonable assumptions, the

first HVSR natural peak gives a reliable estimation of the S-wave resonance frequency of a horizontally layered subsurface (Lachetl & Bard, 1994). Other spectral peaks correspond to a superposition of higher Rayleigh-wave, Love-wave, and S-wave resonance modes (Bonnefoy-Claudet et al., 2008).

The HVSR technique is commonly used to retrieve the site amplification function and its resonance frequency in shallow geological layers (e.g. Lachetl & Bard, 1994; Ibs-von Seht & Wohlenberg, 1999; Fäh et al., 2001, 2008; Bonnefoy-Claudet et al., 2006; Tuan et al., 2011; Panzera et al., 2018; Panzera et al., 2022) and Alpine valleys (Panzera et al. (2022)). It is also deployed to map soft sediment layers and estimate glacier thickness (e.g., Barnaba et al., 2010; Picotti et al., 2017; Preiswerk et al., 2019; Molnar et al., 2022; Seivane et al., 2022). Picotti et al. (2017) applied the HVSR method to five glaciers in the Alpine chain and the west Antarctic ice stream. Their results show how well the resonance frequency in the HVSR spectra correlates with the local bedrock depth over a wide range of ice thicknesses – from a few tens of meters to more than 800 meters. The authors validated their results using other methods, such as GPR, geoelectrical, and active seismic techniques. The limitations of the HVSR method and its reliability for glacier characterization have been addressed in various studies, as reviewed by Picotti et al. (2017) and Molnar et al. (2022). Both groups identify coupling of the sensors with the glacier and the basal impedance contrast as the main controlling factors. Preiswerk et al. (2019) investigated how the glacier's geometry influences the seismic wavefield and reported an azimuth dependence of the HVSR curves' shape. They relate such directivity to higher-order resonance effects caused by the glacier's morphology (like bedrock irregularities). On glaciers, Carcione et al. (2017) demonstrated that attenuation and bedrock deformability affect both frequency and amplitude of HVSR peaks. Moreover, Saenger et al. (2006, 2009) used the HVSR method to extract hydrocarbon maps, focusing on HVSR troughs (or peaks of the inverse – Vertical-to-Horizontal – spectral ratio, noted VHSR) to detect impedance anomalies. Specifically, they reported a peak in the VHSR (typically, values above 1: i.e., vertical energy higher than horizontal energy) at a specific frequency detected by seismic sensors placed above hydrocarbon reservoirs. Similarly, Antunes et al. (2022) noticed that VHSR peaks provides information about seismic energy anomalies generated by fluids in reservoirs since the wavefield is mainly polarized in the vertical direction. They identified a link between the location of the VHSR peak amplitude and the presence of mud and gas inside a volcanic conduit; they also noticed a spatial correlation between

high VHSR anomalies and low resistivity anomalies in geoelectric profiles, corresponding to dome-like reservoirs and associated with high-salinity fluids.

Here, we analyze spectral ratios from ambient seismic noise measured for the Tête-Rousse Glacier (Mont Blanc massif) with the aim of locating potential cavities or areas containing melting water within the glacier. We first present the study area and the seismic data experiment in the field, we next detail the results of spectral analysis obtained from our dense, temporary seismic array. We interpret horizontal polarization of seismic noise around 9 Hz detected by HVSR peaks as the fundamental mode for the whole glacier. Vertical polarization anomalies at higher frequencies detected by HVSR troughs (i.e, more intuitive, VHSR peaks) are considered to reflect reduced basal impedance due to the presence of a cavity or a local anomalous basal response in some areas of the glacier. Results obtained in the field are supported by a proof-of-concept simulation based on the 3D finite-element method.

2 Experimental site and setup

The Tête-Rousse Glacier is located in the Mont Blanc massif in the French Alps (Figure 1*a*), along one of the classic ascension routes (Figure 1b), making it a very popular site among mountaineers. Fed by avalanches in its upper part, this glacier is approximately 450 m long and 150 m wide, with a maximum depth of 80 m, and its surface topography extends from 3100 to 3300 m elevation. There is at least one subglacial water-filled cavity under the central part of the glacier (Vincent et al., 2012), known as the main cavity of this glacier.

In 1892 (July 11), an outburst flood originated from the Tête-Rousse Glacier following collapse of an intraglacial cavity. Around 200 000 m^3 of water and ice were released, dragging about 800 000 m^3 of sediments (boulders, soil, and mud) into the village of Saint Gervais – Le Fayet. The catastrophic event caused 175 fatalities and damaged multiple large infrastructures (Vincent et al., 2010). The mechanism controlling formation and growth of the subglacial cavity has been clearly identified and is probably related to the glacier's thermal regime. According to Vincent et al., 2010), the cold tongue acts as a thermal barrier to water flow. At the time of the outburst flood, factors combined to cause the collapse of the terminal tongue – due to a change in thermal regime (from cold to temperate) or a positive anomaly of the mass balance.

Between 2009 and 2010, data were acquired on the Tête-Rousse Glacier from dense GPR and Surface Nuclear Magnetic Resonance (SNMR) acquisitions. Their analysis revealed a new

subglacial water-filled reservoir measuring 55 000 m^3 (+/- 10 000 m^3) located at a depth of 40 m inside the glacier (Vincent et al., 2012; Legchenko et al., 2014). To prevent another potential outburst flood, the reservoir has been drained artificially (downhole pumps) several times – in 2010, 2011, and 2012 – to prevent the cavity filling up again. In 2013, a large crevasse almost reaching the surface was detected, corresponding to the former cavity roof that collapsed during a pump in 2012. The other few crevasses present on the glacier seem to be the main channel via which water runs into the cavity (Garambois et al., 2016).

From SNMR surveys conducted in 2015 and 2018, no increase in the water content in the main cavity was detected. However, liquid water was detected at several points spread over the upper part of the glacier. These signals could be linked to a water-filled crevasse located upstream from the cavity together with a diffusive zone, revealed using GPR by Garambois et al. (2016) (see Figure S6). These observations suggest a zone where basal partial melting occurs (Gilbert et al., 2012). The glacier is thus in an unsteady state that requires to monitor both its water content and the cavity's geometry.

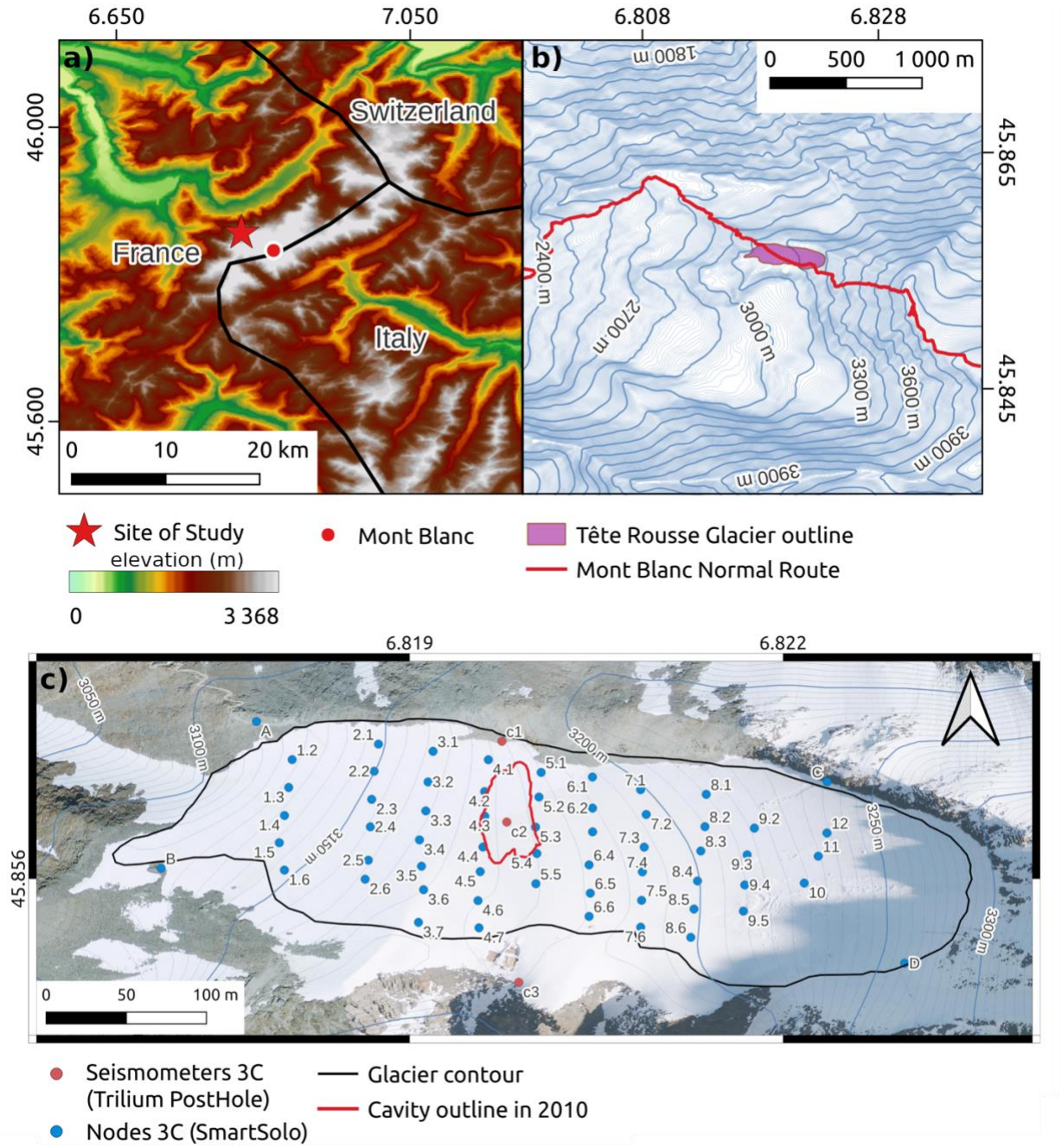

156

157 *Figure 1: a) Mont Blanc massif in the Alps, the red star indicates the position of the Tête-Rousse Glacier. b) outline of the glacier*
158 *and where it crosses the Mont Blanc Normal route. c) 2022 seismic sensor layout.*

159 The seismic acquisition presented in this paper was performed in 2022, from May 4 to 22. We
160 deployed 60 SmartSolo® three-component (3C) 5Hz seismic nodes, in a grid pattern with
161 approximately 30 m by 25 m spacing (Figure 1c). In addition, three 3C Trilium Compact PostHole
162 ® 20s seismometers were installed (named C1 to C3, red dots in Figure 1c), forming a transversal

profile, hence crossing the area above the expected main subglacial cavity (see Supporting Information S1 and Figure S1 for further experimental details).

3 Data analysis and experimental results

We first performed a statistical analysis in the frequency domain for all the signals recorded by the seismic stations over the twenty days of experiment. Results show that the horizontal spectral components have a higher amplitude than the vertical component between 5 Hz and 30 Hz. This is the case over almost the entire seismic array, as expected for glaciers (Preiswerk et al., 2019). HVSR peaks (see Fig. 2a) are expected to reveal the glacier's vibration modes, as reported previously (Picotti et al., 2017; Preiswerk et al., 2019). Additional examples of power density spectrum (PSDs) plots for several sensors can be found in Supporting Information S2 (Fig. S2 and S3). Interestingly, the amplitude of the vertical component is higher than the amplitude of the horizontal component for some seismic sensors at specific frequencies, including sensor C2 located in the central part of the glacier above the expected main cavity (Fig. 2b). Regions where the vertical component dominated (VHSR peaks above 1) are indicative of unusual impedance contrasts at depth, suggesting for instance the presence of cavities or ice/water-related contrasts.

The first HVSR peak recorded by the C2 sensor and most of the nodes is at about 9 Hz (Figure 2a), whereas the first VHSR peak is at about 15 Hz (Figure 2b). We then analyzed how the seismic noise is polarized at these frequencies (see Supporting Information S3 for details). We derived the polarization attributes from singular value decompositions by applying Flinn's method, using the seismic post-processing package Obspy. Our first-pass analysis, between 8 Hz and 10 Hz, encompasses the first mode observed in the HVSR peak (see Figure S4). This analysis reveals high incidence values (often between 75° and 90°), thus horizontal motion of the particle located in C2 in this frequency band. The corresponding azimuth values mostly ranges between 70° and 120° (E-W direction), indicating a longitudinally-oriented horizontal particle motion, in agreement with the directivity of the HVSR peak near 9 Hz (Figure 2a) and the geometry of the glacier. HVSR peak frequency for all other sensors is close to 9 Hz (see Figure S5), with small variability mainly controlled by bedrock depth (Picotti et al., 2017). The azimuth's temporal variability is low, and is probably related to the natural variability of the wavefield propagating in the glacier.

We then looked at the polarization attributes of the data encompassing the first VHSR peak (or HVSR trough) observed - between 14 Hz and 16 Hz (Figure 2a). The seismic signal exhibits a mostly vertical motion of the particle located in C2 (highly variable but with a low incidence value, often between 10° and 50°). The corresponding azimuth values covered all directions, with consistently vertical polarization. The polarization analysis thus confirms our first observations from spectral analysis: the first HVSR peak around 9 Hz corresponds to a horizontal vibration mode along the glacier's main longitudinal axis, whereas the peak around 15 Hz revealed by VHSR peak is mostly in vertical mode. Polarization was stable throughout the duration of recording, adding support to our interpretation that these spectral peaks reflect natural vibration modes of the Tête-Rousse Glacier. These conclusions were further corroborated by the 3D mechanical modeling developed below.

To better locate areas of vertical resonance all over the glacier, we computed the VHSR for each station over the whole time interval, from May 5 to May 21, using a modification of the *hvsrpy* Python tool (Vantassel et al., 2022). We then picked the maximum amplitude averaged over the azimuth within the 2 Hz to 30 Hz frequency range, so as to focus only on first natural modes. Finally, using the ordinary-kriging method (based on a Matern model and a Matheron estimator), we interpolated the VHSR peak amplitude over the whole area covered by the seismic network (Figure 3). This analysis reveals a VHSR below 0.8 for most of the lower part of the glacier, whereas above the fourth line of nodes (see Figure 1c), the VHSR is slightly over 0.8. Moreover, two areas of the glacier were associated with VHSR peaks significantly exceeding 1 (around sensors C2 and 4.1). These areas are consistent with the location of the main subglacial cavity identified in 2010.

In the following section, we describe how we built a simple mechanical 3D model of the glacier to reproduce these resonance modes and their polarization (vertical and horizontal).

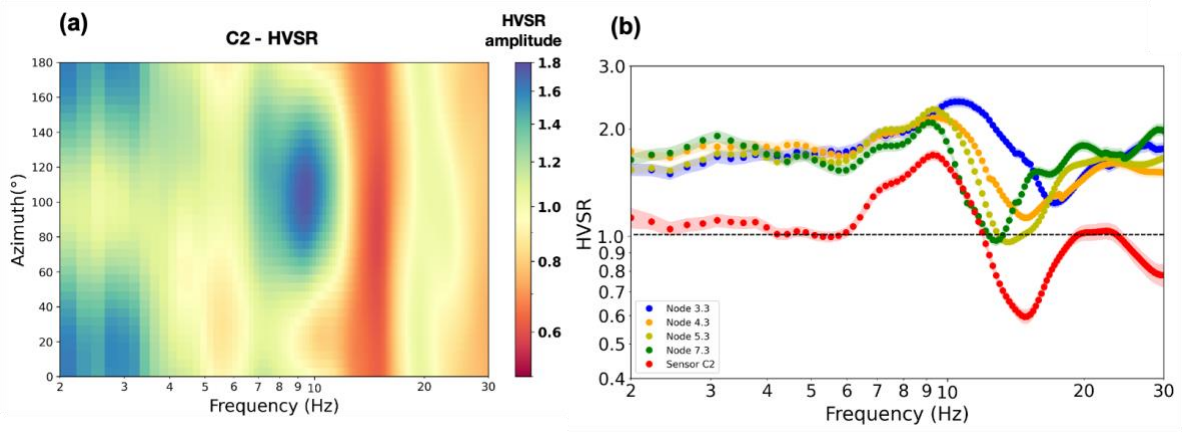

Figure 2: a) Azimuth-dependent HVSR amplitude from seismometer C2 with time-averaging over the whole period of the experiment in May 2022. b) HVSR amplitude from some nodes along a longitudinal line at the center of the glacier, with time- and azimuth- averaging mean amplitude (dots) and standard deviation (errorbars) over the whole period of the experiment in May 2022.

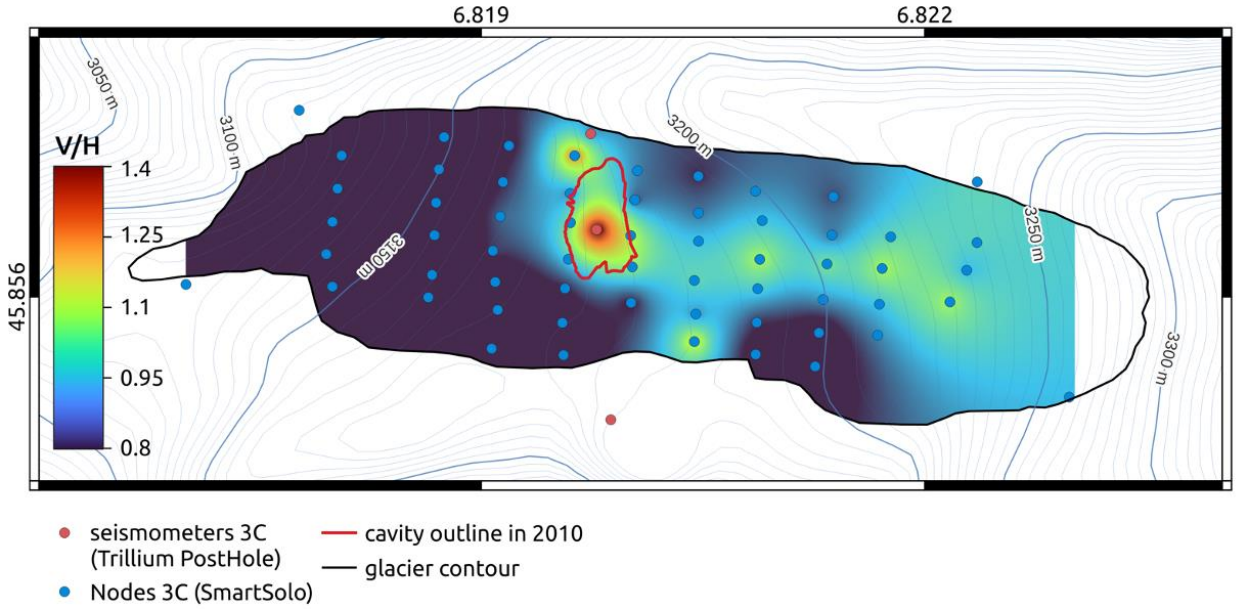

Figure 3: VHSR peak amplitude for the Tête-Rousse Glacier, computed with time- and azimuth-averaging over the whole period of experiment and interpolated by kriging. The cavity outline is deduced from Gagliardini et al. (2011).

4 Numerical validation of results

We performed direct numerical modeling based on finite-element analysis (FEA) to visualize vibrating modes in the Tête-Rousse Glacier and to reconstruct the resonance frequencies along with their modal polarization. We used COMSOL Multiphysics software (Comsol, 2023) for two purposes: 1) to perform modal analysis (MA) of the glacier, solving eigenfrequencies of the 3D object to reproduce the fundamental mode of the whole glacier, and 2) to determine the

frequency response function (FRF) of a 2D axisymmetric model of a local area of the glacier, retrieving the vertical displacements related to the presence of a cavity.

4.1 3D modeling of the horizontal glacier mode

MA computes numerical eigenfrequencies of a solid structure and requires well-constrained structural knowledge of the vibrating object. By combining all GPR and borehole measurements, Garambois et al. (2016) produced a well-resolved estimation of the ice-bedrock interface's topography (see Figure S6). For our model, we simplified the 3D geometry of the glacier to an ellipsoid-shaped ice block with dimensions matching the field observations, lying on a rigid bedrock. Our modeled solid is composed of 94 000 quadratic tetrahedral finite elements, with a maximum dimension of 15 m. We applied consistent boundary conditions to mimic the configuration of the site: embedding the sides of the stable bedrock far from the glacier body, and leaving the upper surface free. The mechanical parameters of both glacier and bedrock were estimated from the literature for ice and fractured moraine (Sergeant et al., 2020; Table S1). For the sake of simplicity, the properties of both glacier and bedrock were assumed to be homogeneous.

We found the first eigenfrequency, corresponding to the fundamental mode, to be at 9.42 Hz (Figure 4a), close to the experimental HVSR peak measured at most nodes – at around 9 Hz (Figure 2a). This first mode is a flexural mode polarized along the longest axis of the glacier (the longitudinal direction). The polarization of this first numerical mode is consistent with the observed directivity of the 9 Hz HVSR peak measured by most of the seismic sensors around the 100° azimuth. We noted that observed HVSR peak frequencies show a spatial variability over the glacier (Figure S5 in Supplementary Materials), mainly depending on the local bedrock interface depth and crevasses. We actually measured local "pseudo-modes" of compartments of the glacier, rather than a global resonance of the whole glacier, due to the attenuation on the glacier that could not be addressed by the model. Nevertheless, this 3D model suggests a longitudinal resonance around 9 Hz, similar to local horizontal modes detected by HVSR peaks.

Overall, this MA validates to the first order the mechanical parameters set of the ice and the bedrock and our interpretation of horizontal modes detected by HVSR. Then, a 2D modeling is needed to accurately interpretate local vertical resonance modes detected by VHSR peaks.

4.2 2D modeling of the cavity mode

We then focused on the presence of a subglacial cavity to assess its effects on spectral analysis. For simplicity, we used a 2D geometry with vertical axial symmetry, focusing on the central part of the glacier. We assumed the simulated subglacial water-filled cavity to be elliptical, with realistic dimensions. We only constrained the bedrock depth at 75 m and the location of the top of the cavity at around 35 m depth, in line with GPR measurements obtained in 2022 (Figure 4b). Our 2D solid model was composed of 12 000 quadratic tetrahedral finite elements, with a maximum size of 3 m side. A mesh refinement provided greater than 1% precision for all the mechanical fields computed below 30 Hz (minimum of 20 elements per wavelength). Acoustoelastic coupling between liquid water and ice was implemented by imposing continuous normal acceleration at the cavity interface. We simulated ambient seismic sources by applying a linear harmonic loading between 5 Hz and 20 Hz along a horizontal line crossing the geometry. After computing the FRF, we retrieved the corresponding frequency-dependent response displacement in the vertical direction at several points on the surface (closely reproducing the positions at which seismic recordings were made by a vertical seismometer).

We compared the vertical displacements (along the Z-axis) obtained with and without the subglacial cavity in Figure 4c. For a simulated sensor placed right above it, vertical vibrations has a clearly larger amplitude when the cavity is present. In these conditions, the peak amplitude was two-fold that measured without the cavity, and has a slightly different frequency.

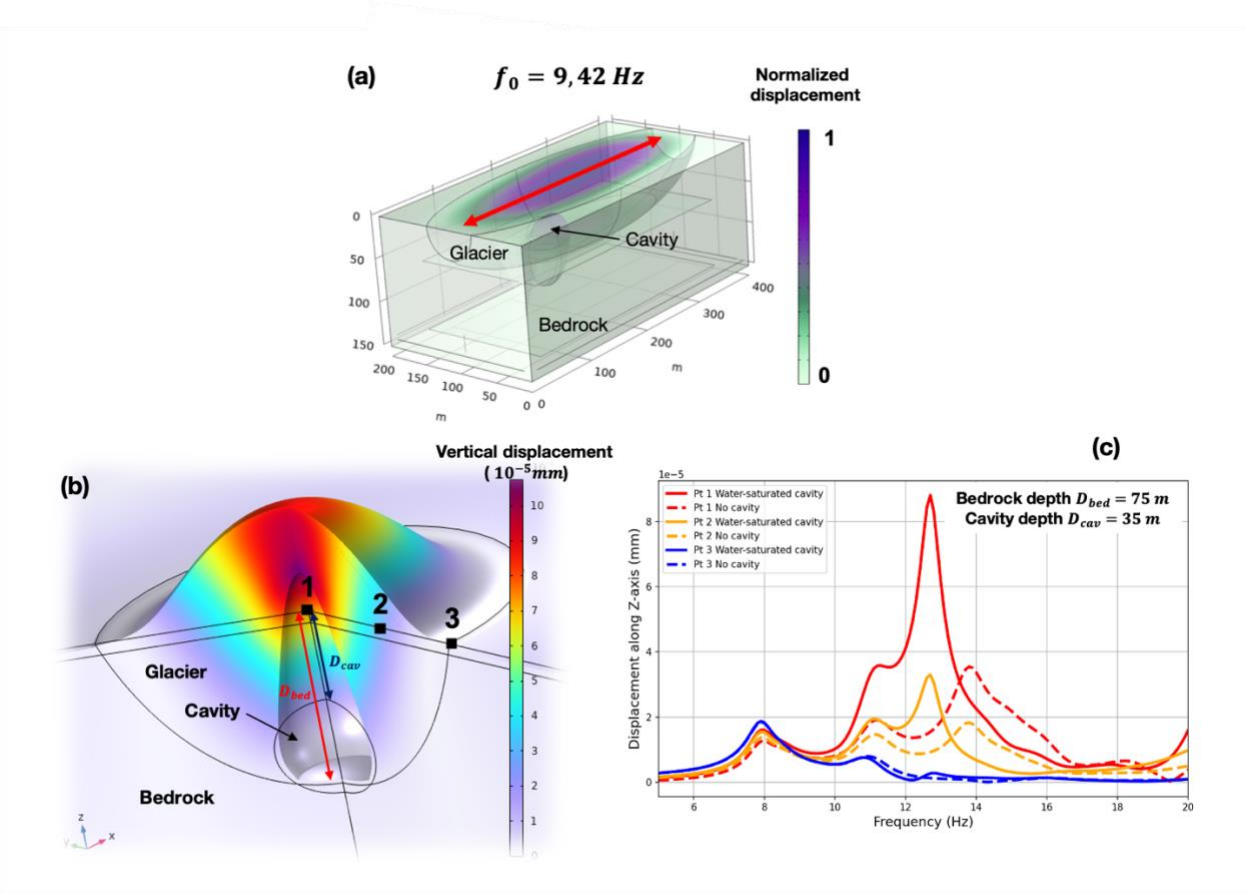

Figure 4: Fundamental mode of the glacier, based on the MA of the mechanical model applying simple elliptic geometry adapted from a). The main direction of displacement is depicted by the red arrow. (b) Vertical displacement of the 2D axisymmetric mechanical model at 12.8 Hz, showing the location of points 1, 2, and 3 at the glacier's surface. (c) Vertical displacement occurring at points 1, 2, and 3, recorded between 5 and 20 Hz with the cavity (continuous lines) and without the cavity (dashed lines), as outputs of FRF.

5 Discussion

The aim of this study was to analyze ambient noise data from the Tête-Rousse Glacier to verify whether it could be used to detect and monitor subglacial cavities. Findings were confirmed by modeling. The results presented in Figure 3 identify two hotspots with high (above 1.1) VHSR amplitude peaks in the central part of the glacier. The first hotspot (centered around the C2 sensor) corresponds to the center of the main cavity first detected in 2010, and confirmed in 2018 using GPR and by borehole drilling (Figure S6). The second one was measured only by node 4.1, which corresponds to the area above the 2010 cavity, but with a more limited lateral extension. This sensor was also the closest to a transversal crevasse identified on the glacier's right bank, known as the former roof of the cavity that collapsed in 2012 (Garambois et al., 2016). Note that this crevasse cannot explain the VHSR amplitude peak, since we expect an exacerbated horizontal

297 energy increase at the border of the subvertical crack, due to shear vibration modes. However, this
298 crevasse was previously shown to feed the cavity with surface water (Garambois et al., 2016).
299 These recent observations may then result from a reshaping of the central cavity into two (or more)
300 independent smaller cavities. Additional geophysical observations will be required to confirm this
301 hypothesis.
302 Downward from the cavity line, the VHSR amplitude is always lower than 0.8 (Figure 3). This
303 area corresponds to the cold part of the glacier (Gilbert et al., 2012; Garambois et al., 2016), where
304 the basal ice temperature is always much lower than that of the melting point, so that the ice layer
305 sticks to the underlying bedrock and no basal melting water is expected.
306 Upward from the cavity line, the VHSR amplitude generally stands between 0.8 and 1.1. This area
307 is very well spatially correlated with the temperate area of the glacier (Gilbert et al., 2012;
308 Garambois et al., 2016), where the basal ice temperature remains at the fusion point, allowing
309 liquid water to emerge at the ice-bedrock interface, and some detachments to occur locally.
310 Moreover, within the temperate ice, a large amount of liquid water was detected by SNMR (Figure
311 S6). No large cavity containing liquid water has been revealed by GPR up to now, but small diffuse
312 cavities filled with liquid water, or wet patches, may exist within this volume, generating slight
313 vertical vibrations. These results confirm the general basal conditions of the glacier, as already
314 suggested by GPR and SNMR surveys.
315 The interpretation of VHSR amplitude has to be performed carefully, mainly due to the temporal
316 variability of the seismic noise, the presence of body and surface waves in the wavefield, and local
317 2D or 3D resonance effects. In this study, threshold values delineating melting areas have been set
318 with the help of prior information on Tête-Rousse Glacier. Hence, it is worth noting than VHSR
319 amplitude values are site-dependent, and conclusions based on this proxy should not yet be
320 definitive without additional information.
321 It should also be noted that this seismic experiment was probably oversized: a shorter-lived, less
322 intensive survey could have provided similar results. Statistical analysis of the temporal variability
323 of the measurements will be the subject of further work, but at this point we estimate that only a
324 few days of ambient noise data is required to conduct this type of experiment on glaciers. This
325 duration might be decreased to a few hours through optimization of the data processing procedure.
326 Among other advanced techniques, the extraction of Rayleigh wave ellipticity by DOP-E method
327 (Berbellini et al., 2019; Jones et al., 2023) and its inversion may significantly improve the

identification of englacial features (see Supporting Information S6 and Figure S7 for further details).

6 Conclusion

The spectral analysis performed on continuous seismic records acquired at the surface of the Tête-Rousse Glacier exhibits both a HVSR frequency peak and a polarization that corresponds to the first longitudinal mode of the glacier, confirming the elastic parameters of ice and bedrock. The VHSR exhibits a clear positive anomaly indicating the presence of a subglacial cavity (areas where VHSR > 1.1) at a location that is consistent with the known position of the cavity. However, the VHSR mapping suggests that the cavity's geometry had been modified since previous observations, dating from 2010 and 2018. In addition, the upper part of the glacier, known to be composed of temperate ice, shows VHSR values close to 1, indicating a possible role for diffuse liquid water content and/or local detachment of the basal ice from the bedrock. These results indicate that ambient seismic noise-based spectral analysis of data collected by sensors at the surface can be used to map the presence of potential cavities in glaciers. Computing VHSR amplitude peaks is very straightforward, making this method accessible and rapid. But the level at which VHSR can detect cavities depends on the impedance contrast between the ice and the underlying layer (fractured or intact bedrock, sediments), and will need further investigation to be applicable on glaciers without prior information on their subglacial conditions.

Acknowledgments

The authors wish to thank Sisprobe for renting their SmartSolo nodes and for assistance with data management. The three Centaur & Trillium PH sensors were from the CNRS-INSU-SISMOB pool. The authors gratefully acknowledge experimental help from Simon Bonin, Baptiste Camus, and Agnès Helmstetter. This work was partially funded by the French Ministère de la Transition écologique et de la Cohésion des territoires (Ministry for Ecological Transition and Territorial Cohesion) through its DGPR ROGP program, by the French national research agency (ANR) through its "Plan de Relance" program, and by the Engineering-Consultancy Bureau Géolithe.

Open Research

Data from seismic stations C1, C2, and C3 are available on RESIF (https://seismology.resif.fr/networks/#/YZ__2022).

Seismic data from nodes are temporarily available on ScienceDB through this link (https://www.scidb.cn/s/faUZf2), before being available permanently on RESIF.

References

Antunes, V., Planès, T., Obermann, A., Panzera, F., D'amico, S., Mazzini, A., Sciarra, A., Ricci, T., Matteo Lupi, 2022. Insights into the dynamics of the Nirano Mud Volcano through seismic characterization of drumbeat signals and V/H analysis. J. Volcanol. Geotherm. Res. 431, 107619.

Barnaba, C., Marello, L., Vuan, A., Palmieri, F., Romanelli, M., Priolo, E., Braitenberg, C., 2010. The buried shape of an alpine valley from gravity surveys, seismic and ambient noise analysis. Geophys. J. Int. 180, 715–733.

Berbellini, A., Schimmel, M., Ferreira, A. M., & Morelli, A. (2019). Constraining S-wave velocity using Rayleigh wave ellipticity from polarization analysis of seismic noise. *Geophysical Journal International*, *216*(3), 1817-1830

Björnsson, H., 1998. Hydrological characteristics of the drainage system beneath a surging glacier. Nature 395, 771–774.

Bonnefoy-Claudet, S., Cotton, F., Bard, P.-Y., 2006. The nature of noise wavefield and its applications for site effects studies. Earth-Sci. Rev. 79, 205–227.

Bonnefoy-Claudet, S., Köhler, A., Cornou, C., Wathelet, M., Bard, P.-Y., 2008. Effects of Love Waves on Microtremor H/V Ratio. Bull. Seismol. Soc. Am. 98, 288–300.

Boon, S., Sharp, M., 2003. The role of hydrologically-driven ice fracture in drainage system evolution on an Arctic glacier. Geophys. Res. Lett. 30.

Breien, H., De Blasio, F.V., Elverhøi, A., Høeg, K., 2008. Erosion and morphology of a debris flow caused by a glacial lake outburst flood, Western Norway. Landslides 5, 271–280.

Carcione, J.M., Picotti, S., Francese, R., Giorgi, M., Pettenati, F., 2017. Effect of soil and bedrock anelasticity on the S-wave amplification function. Geophys. J. Int. 208, 424–431.

Cenderelli, D.A., Wohl, E.E., 2003. Flow hydraulics and geomorphic effects of glacial-lake outburst floods in the Mount Everest region, Nepal. Earth Surf. Process. Landf. 28, 385–407.

Fäh, D., Kind, F., Giardini, D., 2001. A theoretical investigation of average H/V ratios. Geophys. J. Int. 145, 535–549.

Fäh, D., Stamm, G., Havenith, H.-B., 2008. Analysis of three-component ambient vibration array measurements. Geophys. J. Int. 172, 199–213.

Flinn, E., 1965. Signal analysis using rectilinearity and direction of particle motion. IEEE 53, 1874–1876.

Fountain, A.G., Walder, J.S., 1998. Water flow through temperate glaciers. Rev. Geophys. 36, 299–328.

Gagliardini, O., Gillet-Chaulet, F., Durand, G., Vincent, C., Duval, P., 2011. Estimating the risk of glacier cavity collapse during artificial drainage: The case of Tête Rousse Glacier. Geophys. Res. Lett. 38.

Garambois, S., Legchenko, A., Vincent, C., Thibert, E., 2016. Ground-penetrating radar and surface nuclear magnetic resonance monitoring of an englacial water-filled cavity in the polythermal glacier of Tête Rousse. Geophysics 81, WA131–WA146.

Gilbert, A., Vincent, C., Wagnon, P., Thibert, E., Rabatel, A., 2012. The influence of snow cover thickness on the thermal regime of Tête Rousse Glacier (Mont Blanc range, 3200 m a.s.l.): Consequences for outburst flood hazards and glacier response to climate change. J. Geophys. Res. Earth Surf. 117.

Gimbert, F., Nanni, U., Roux, P., Helmstetter, A., Garambois, S., Lecointre, A., Walpersdorf, A., Jourdain, B., Langlais, M., Laarman, O., Lindner, F., Sergeant, A., Vincent, C., Walter, F., 2021. A Multi-Physics Experiment with a Temporary Dense Seismic Array on the Argentière Glacier, French Alps: The RESOLVE Project. Seismol. Res. Lett. 92, 1185–1201.

Haeberli, W., 1983. Frequency and Characteristics of Glacier Floods in the Swiss Alps. Ann. Glaciol. 4, 85–90.

Haeberli, W., Kääb, A., Mühll, D.V., Teysseire, P., 2001. Prevention of outburst floods from periglacial lakes at Grubengletscher, Valais, Swiss Alps. J. Glaciol. 47, 111–122.

Haeberli, W., Kääb, A., Paul, F., Chiarle, M., Mortara, G., Mazza, A., Deline, P., Richardson, S., 2002. A surge-type movement at Ghiacciaio del Belvedere and a developing slope instability in the east face of Monte Rosa, Macugnaga, Italian Alps. Nor. Geogr. Tidsskr. - Nor. J. Geogr.

Haeberli, W., Müller, P., Alean, P., Bösch, H., 1989. Glacier Changes Following the Little Ice Age — A Survey of the International Data Basis and Its Perspectives. In: Glacier Fluctuations and Climatic Change. Springer, Dordrecht, pp. 77–101.

Harper, J.T., Bradford, J.H., Humphrey, N.F., Meierbachtol, T.W., 2010. Vertical extension of the subglacial drainage system into basal crevasses. Nature 467, 579–582.

Helmstetter, A., Moreau, L., Nicolas, B., Comon, P., Gay, M., 2015b. Intermediate-depth icequakes and harmonic tremor in an Alpine glacier (Glacier d'Argentière, France): Evidence for hydraulic fracturing? J. Geophys. Res. Earth Surf. 120, 402–416.

Helmstetter, A., Nicolas, B., Comon, P., Gay, M., 2015. Basal icequakes recorded beneath an Alpine glacier (Glacier d'Argentière, Mont Blanc, France): Evidence for stick-slip motion? J. Geophys. Res. Earth Surf. 120, 379–401.

Jones, J.P., Eaton, D.W., Caffagni, E., 2016. Quantifying the similarity of seismic polarizations. Geophys. J. Int. 204, 968–984.

Jones, G. A., Ferreira, A. M. G., Kulessa, B., Schimmel, M., Berbellini, A., & Morelli, A. (2023). Constraints on the cryohydrological warming of firn and ice in Greenland from Rayleigh wave ellipticity data. *Geophysical Research Letters*, *50*(15), e2023GL103673

Jurkevics, A., 1988. Polarization analysis of three-component array data. Bull. Seismol. Soc. Am. 78, 1725–1743.

Kattelmann, R., 2003. Glacial Lake Outburst Floods in the Nepal Himalaya: A Manageable Hazard? Nat. Hazards 28, 145–154.

Kershaw, J.A., Clague, J.J., Evans, S.G., 2005. Geomorphic and sedimentological signature of a two-phase outburst flood from moraine-dammed Queen Bess Lake, British Columbia, Canada. Earth Surf. Process. Landf. 30, 1–25.

Konno, K., Ohmachi, T., 1998. Ground-motion characteristics estimated from spectral ratio between horizontal and vertical components of microtremor. Bull. Seismol. Soc. Am. 88, 228–241.

Lachetl, C., Bard, P.-Y., 1994. Numerical and Theoretical Investigations on the Possibilities and Limitations of Nakamura's Technique. J. Phys. Earth 42, 377–397.

Legchenko, A., Vincent, C., Baltassat, J.M., Girard, J.F., Thibert, E., Gagliardini, O., Descloitres, M., Gilbert, A., Garambois, S., Chevalier, A., Guyard, H., 2014. Monitoring water accumulation in a glacier using magnetic resonance imaging. The Cryosphere 8, 155–166.

Molnar, S., Sirohey, A., Assaf, J., Bard, P.-Y., Castellaro, S., Cornou, C., Cox, B., Guillier, B., Hassani, B., Kawase, H., Matsushima, S., Sánchez-Sesma, F.J., Yong, A., 2022. A review of the microtremor horizontal-to-vertical spectral ratio (MHVSR) method. J. Seismol. 26, 653–685.

Nakamura, Y., 1989. A METHOD FOR DYNAMIC CHARACTERISTICS ESTIMATION OF SUBSURFACE USING MICROTREMOR ON THE GROUND SURFACE. Railw. Tech. Res. Inst. Q. Rep. 30.

Nanni, U., Gimbert, F., Roux, P., Lecointre, A., 2021. Observing the subglacial hydrology network and its dynamics with a dense seismic array. Proc. Natl. Acad. Sci. 118, e2023757118.

Nanni, U., Roux, P., Gimbert, F., Lecointre, A., 2022. Dynamic Imaging of Glacier Structures at High-Resolution Using Source Localization With a Dense Seismic Array. Geophys. Res. Lett. 49, e2021GL095996.

Nogoshi, M., Igarashi, T., 1971. On the amplitude characteristics of ambient noise (part 2). J Seism. Soc Jpn 24, 26–40.

437 Panzera, F., Alber, J., Imperatori, W., Bergamo, P., Fäh, D., 2022. Reconstructing a 3D model from geophysical data for local
438 amplification modelling: The study case of the upper Rhone valley, Switzerland. Soil Dyn. Earthq. Eng. 155, 107163.

439 Panzera, F., D'amico, S., Lupi, M., Mauri, G., Karyono, K., Mazzini, A., 2018. Lusi hydrothermal structure inferred through
440 ambient vibration measurements. Mar. Pet. Geol. 90, 116–124.

441 Petrenko, V.F., Whitworth, R.W., 2002. Physics of ice. Oxf. Univ. Press 373 pp.

442 Picotti, S., Francese, R., Giorgi, M., Pettenati, F., Carcione, J.M., 2017. Estimation of glacier thicknesses and basal properties
443 using the horizontal-to-vertical component spectral ratio (HVSR) technique from passive seismic data. J. Glaciol. 63, 229–248.

444 Preiswerk, L.E., Michel, C., Walter, F., Fäh, D., 2019. Effects of geometry on the seismic wavefield of Alpine glaciers. Ann.
445 Glaciol. 60, 112–124.

446 Roberts, M.J., 2005. JÖkulhlaups: A reassessment of floodwater flow through glaciers. Rev. Geophys. 43.

447 Saenger, E.H., Schmalholz, S.M., Lambert, M.-A., Nguyen, T.T., Torres, A., Metzger, S., Habiger, R.M., Müller, T., Rentsch, S.,
448 Méndez-Hernández, E., 2009. A passive seismic survey over a gas field: Analysis of low-frequency anomalies. Geophysics 74,
449 O29–O40.

450 Saenger, E.H., Torres, A., Rentsch, S., Lambert, M., Schmalholz, S.M., Mendez-Hernandez, E., 2006. A hydrocarbon microtremor
451 survey over a gas field: Identification of seismic attributes | SEG Technical Program Expanded Abstracts 2007. SEG Tech.
452 Program Expand. Abstr.

453 Seht, M.I., Wohlenberg, J., 1999. Microtremor measurements used to map thickness of soft sediments. Bull. Seismol. Soc. Am.

454 Seivane, H., García-Jerez, A., Navarro, M., Molina, L., Navarro-Martínez, F., 2022. On the use of the microtremor HVSR for
455 tracking velocity changes: a case study in Campo de Dalías basin (SE Spain). Geophys. J. Int. 230, 542–564.

456 Sergeant, A., Chmiel, M., Lindner, F., Walter, F., Roux, P., Chaput, J., Gimbert, F., Mordret, A., 2020. On the Green's function
457 emergence from interferometry of seismic wave fields generated in high-melt glaciers: implications for passive imaging and
458 monitoring. The Cryosphere 14, 1139–1171.

459 Tuan, T.T., Scherbaum, F., Malischewsky, P.G., 2011. On the relationship of peaks and troughs of the ellipticity (H/V) of Rayleigh
460 waves and the transmission response of single layer over half-space models. Geophys. J. Int. 184, 793–800.

461 Vantassel, J.P., 2020. jpvantassel/hvsrpy: latest (Concept). Zenodo. http://doi.org/10.5281/zenodo.3666956

462 Vidale, J.E., 1986. Complex polarization analysis of particle motion. Bull. Seismol. Soc. Am. 76, 1393–1405.

463 Vilímek, V., Zapata, M.L., Klimeš, J., Patzelt, Z., Santillán, N., 2005. Influence of glacial retreat on natural hazards of the
464 Palcacocha Lake area, Peru. Landslides 2, 107–115.

465 Vincent, C., Descloitres, M., Garambois, S., Legchenko, A., Guyard, H., Gilbert, A., 2012. Detection of a subglacial lake in Glacier
466 de Tête Rousse (Mont Blanc area, France). J. Glaciol. 58, 866–878.

467 Vincent, C., Garambois, S., Thibert, E., Lefèbvre, E., Meur, E.L., Six, D., 2010. Origin of the outburst flood from Glacier de Tête
468 Rousse in 1892 (Mont Blanc area, France). J. Glaciol. 56, 688–698.

469 Vincent, C., Thibert, E., Gagliardini, O., Legchenko, A., Gilbert, A., Garambois, S., Condom, T., Baltassat, J.M., Girard, J.F., 2015.
470 Mechanisms of subglacial cavity filling in Glacier de Tête Rousse, French Alps. J. Glaciol. 61, 609–623.

471 Wathelet, M., Chatelain, J.-L., Cornou, C., Giulio, G.D., Guillier, B., Ohrnberger, M., Savvaidis, A., 2020. Geopsy: A User-Friendly
472 Open-Source Tool Set for Ambient Vibration Processing. Seismol. Res. Lett. 91, 1878–1889.

473 Werder, M.A., Bauder, A., Funk, M., Keusen, H.-R., 2010. Hazard assessment investigations in connection with the formation of
474 a lake on the tongue of Unterer Grindelwaldgletscher, Bernese Alps, Switzerland. Nat. Hazards Earth Syst. Sci. 10, 227–237.

475 Withers, M., Aster, R., Young, C., Beiriger, J., Harris, M., Moore, S., Trujillo, J., 1998. A comparison of select trigger algorithms
476 for automated global seismic phase and event detection. Bull. Seismol. Soc. Am. 88, 95–106.